

Quantum Bayesian Optimization for Quality Improvement in Fuselage Assembly

Jiayu Liu^a, Chong Liu^b, Trevor Rhone^c, and Yinan Wang^a

Emails: {liuj35, rhonet, wangy88}@rpi.edu, cliu24@albany.edu

^a Department of Industrial and Systems Engineering, Rensselaer Polytechnic Institute

^b Department of Computer Science, University at Albany, State University of New York

^c Department of Physics, Applied Physics & Astronomy, Rensselaer Polytechnic Institute

Abstract

Recent efforts in smart manufacturing have enhanced aerospace fuselage assembly processes, particularly by innovating shape adjustment techniques to minimize dimensional gaps between assembled sections. Existing approaches have shown promising results but face the issue of low sample efficiency from the manufacturing systems. It arises from the limitation of the classical Monte Carlo method when uncovering the mean response from a distribution. In contrast, recent work has shown that quantum algorithms can achieve the same level of estimation accuracy with significantly fewer samples than the classical Monte Carlo method from distributions. Therefore, we can adopt the estimation of the quantum algorithm to obtain the estimation from real physical systems (distributions). Motivated by this advantage, we propose a Quantum Bayesian Optimization (QBO) framework for precise shape control during assembly to improve the sample efficiency in manufacturing practice. Specifically, this approach utilizes a quantum oracle, based on finite element analysis (FEA)-based models or surrogate models, to acquire a more accurate estimation of the environment response with fewer queries for a certain input. QBO employs an Upper Confidence Bound (UCB) as the acquisition function to strategically select input values that are most likely to maximize the objective function. It has been theoretically proven to require much fewer samples while maintaining comparable optimization results. In the case study, force-controlled actuators are applied to one fuselage section to adjust its shape and reduce the gap to the adjoining section. Experimental results demonstrate that QBO achieves significantly lower dimensional error and uncertainty compared to classical methods, particularly using the same queries from the simulation.

Keywords: Fuselage Assembly; Bayesian Optimization; Quantum Computing

1 Introduction

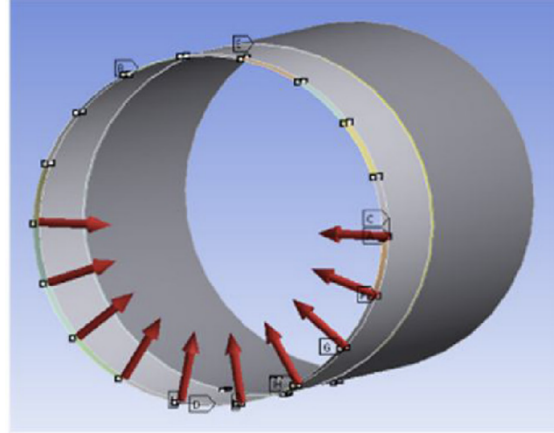
Over the past century, the materials utilized in the aerospace industry have evolved from traditional wood and metal to advanced composite materials. Composite materials, such as fiberglass-reinforced plastics, offer substantial benefits over their predecessors. These

advantages include a higher specific modulus, exceptional corrosion resistance, and ease of manufacturing. In recent aerospace manufacturing, large foundational components are first produced and subsequently assembled to construct an entire aircraft. For instance, multiple fuselage sections are manufactured independently in the factory and subsequently joined together. A critical challenge during this assembly process is the presence of mismatches between the sections being joined. These dimensional errors can critically undermine the structural stability of the aircraft. Therefore, precise shape control is crucial to maintaining the integrity and reliability of the aerospace industry.

Shape control during fuselage assembly typically involves the installation of force-controlled actuators placed along the edges of fuselage sections to correct shape distortions by applying either pulling or pushing forces. The optimal number and positioning of these actuators are determined through experimental design procedures. Fig. 1 provides a schematic illustration of the shape adjustment, highlighting how one fuselage section remains fixed while the adjacent section is precisely aligned using multiple isometric actuators. These actuators are adjusted to minimize the gaps between sections, with their forces set in the radial direction within the fuselage’s coordinate system either inward (push) or outward (pull).



(a) Force-controlled actuators



(b) Fixture layout

Figure 1: Schemes of (a) force-controlled actuators system and (b) fixtures in fuselage assembly (Wen et al., 2018).

Identifying the optimal placements and forces of actuators in fuselage assembly is chal-

lenging due to several reasons. (i) In real-world manufacturing, the high cost of experimentation makes it impractical to collect an extensive number of data points to explore different plans of actuator placements and forces. Alternatively, a simulated environment (i.e., based on finite element analysis – FEA) can be created to replicate the change in fuselage shape in response to various actuator placements and forces. However, even in simulation, estimating shape mismatch using FEA is highly time-consuming, especially when a large number of samples are evaluated. (ii) The solutions are usually non-unique. This property implies that multiple force configurations can yield identical deviations. Hence, there is no assurance of finding only one globally optimal solution. (iii) Real manufacturing conditions involve measurement noise, including errors from sensors, calibration drift, temperature-induced deformation, etc. The measurement noise introduced uncertainty for the response (i.e., measured shape deformation) with the same set of input (placement and forces), which can significantly impact the efficiency in identifying the optimal placements and forces of actuators.

Several existing methodologies have partially addressed these challenges. For the first challenge, Yue et al. (2018) proposed several surrogate models as a computationally efficient alternative to the FEA-based approach. These surrogate models include various uncertainties as an approximation to shape deviations, significantly reducing computational resources and analysis time compared to conventional FEA methods. However, it does not fundamentally resolve the issue of sample-demanding identifying the optimal placements and forces of actuators. Addressing the variability in initial shapes, reinforcement learning methods have also been explored. Lutz et al. (2024) developed an agent trained on extensive fuselage assembly scenarios, enabling it to generalize effectively across different initial shape conditions without iteratively finding optimal solutions for each case. However, training such an agent is time-consuming and requires extensive datasets with diverse initial shapes, making the process both sample-inefficient and computationally costly (There are 1500 conditions, and each condition takes 20,000 queries to train). Alternatively, Bayesian Optimization (BO) has been investigated for actuator placement and shape control in fuselage assembly (AlBahar et al., 2022, 2023). Unlike Reinforcement Learning (RL), BO does not require pretraining on large datasets. Instead, it directly searches for optimal solutions in a case-by-case manner by sequentially selecting new evaluations. This makes BO par-

ticularly popular in manufacturing settings. In addition, RL for fuselage assembly (Lutz et al., 2024) is performed under the assumption that the measurement collected from the manufacturing system is noise-free, which does not hold in practice. Its performance under noisy observations is still awaiting investigation.

Improving sample efficiency remains a crucial long-term objective in manufacturing, with the benefit of reducing computational costs and economic investment in quality improvement. It has been proven that BO has a theoretical bound on both *cumulative regret* and *simple regret*. Specifically, cumulative regret measures the sum of the differences between the observations and the optimal outcome over T queries, whereas simple regret measures the difference between the best observation and the optimal outcome after T queries. In this paper, we focus on the concept of cumulative regret. With a total of T queries, the lower bound for cumulative regret is $\Omega(\sqrt{T})$ (Scarlett et al., 2017) (ignoring log factor), which guarantees the finding of the global optimum within a certain precision. Nevertheless, BO still requires a substantial number of queries to estimate the minimum deviation. Thus, a notable research gap exists in efficiently identifying optimal solutions with fewer queries.

Current research works have shown that the quantum algorithm of Monte Carlo estimation achieves quadratic speedup to estimate the mean from a distribution with the same precision (Montanaro, 2015) compared with classic mean estimation. Leveraging these findings, Quantum Bayesian Optimization has been developed for sample efficiency, which achieves the upper bound for cumulative regret $O(\text{poly log } T)$ (Dai et al., 2023). Inspired by that, we adapted a Quantum Bayesian Optimization (QBO) framework specifically designed for the fuselage assembly. Our method effectively addresses the critical challenge for sample efficiency: by employing quantum algorithms, our approach achieves optimal solutions with fewer queries compared to classical algorithms. Our proposed QBO framework follows a similar pattern to the classical BO. The major subroutine of QBO is Quantum Monte Carlo (Sec. 3.3.3) estimation, which plays a key role in estimating the mean response of the objective function given a specific input. In addition, the framework uses an acquisition function to guide the selection of input values so that the posterior of the surrogate model can be iteratively updated and then find potential solutions.

We summarize our contributions as follows:

- This work is the first trial to demonstrate quantum advantage in optimization for manufacturing process design and quality improvement.
- The proposed method demonstrates superior sample efficiency in experiments on fuselage assembly processes compared with classic Bayesian Optimization.

The paper is organized in the following ways: Sec. 2 briefly summarize the work related fuselage assembly. Sec. 3 introduces our proposed method. Sec. 4 presents our experimental settings and results. Finally, Sec. 5 summarizes the finding in the paper.

In this paper, the concept of samples is the same as that of queries and iterations. We use the words interchangeably.

2 Related Work

In manufacturing, the problem of design and optimization is usually formulated as finding the optimal solution over the design space. Intuitively, it is solved via the interaction between a “solver” and an “environment”. The role of the “solver” is to generate different designs strategically, and the role of the “environment” is to quantitatively evaluate a specific design as feedback to the “solver”. Designing and optimizing manufacturing processes often involves iteratively exploring a large solution space while balancing accuracy, cost, and robustness. In fuselage assembly, achieving precise shape control requires both accurate simulation of structural responses and minimizing the number of measurements in a noisy environment. These challenges motivate researchers to seek advanced algorithms. Recent studies indicate that quantum algorithms can achieve accuracy and sample efficiency comparable to, or even exceeding, those of classical methods in certain manufacturing tasks. In this section, we review related works in two parts. (i) methods for quality control and optimization in fuselage assembly processes, and (ii) quantum algorithms that offer potential advantages for computationally intensive simulation and optimization tasks in the industry or related field.

2.1 Quality Control in Aircraft Assembly Process

Recently, significant research efforts have been dedicated to the topic of fuselage assembly process for composite materials. Wen et al. (2019) proposed a finite element analysis (FEA) method that was groundbreaking because it virtually simulated the assembly process of two composite fuselage sections, providing detailed stress analysis resulting from actuator-applied forces. To account for uncertainties during shape control, Yue et al. (2018) developed a surrogate model that significantly enhanced the accuracy of simulations. Further addressing the computational intensity associated with surrogate modeling, Zhong et al. (2022) introduced a novel FEA framework specifically designed for shape control applications in fuselage assembly.

Besides virtual environments based on surrogate and FEA-based models, optimization methods have drawn considerable interest for determining optimal actuator forces to minimize dimensional gaps. Du et al. (2019) constructed a linear model capturing the relationship between applied actuator forces and shape deviations, proposing an optimization-based approach for gap minimization. Expanding on this work, Du et al. (2022) introduced a sparse learning model with loss l_∞ , further achieving smaller dimensions for fuselage assemblies. In addition to optimization methods, reinforcement learning and BO methods (Lutz et al., 2024; AlBahar et al., 2023) have also been explored for reducing gaps. Mou et al. (2023) introduced a sparse sensor to perform adaptive control, which aims to improve the shape control performance. In this paper, we address two significant limitations that remain among these methods: (i) as these approaches typically assume noise-free conditions, which is unrealistic for real-world manufacturing scenarios; (ii) these methods require a sufficiently large amount of samples to find the optimal solutions.

2.2 Quantum Algorithms in Advanced Manufacturing

Advanced simulation techniques, such as the finite element method (FEM), have been investigated and developed as the “environment” (Wang et al., 2024), and optimization methods, such as mathematical programming, have been proposed as the “solver” (Wang and Yue, 2012). From the “environment” perspective, compared with its classical counterpart, quantum computing has enhanced the simulation capabilities of scientific comput-

ing, particularly in developing general linear algebra routines (a core subroutine in FEM) (Clader et al., 2013; Montanaro and Pallister, 2016). The linear system is ubiquitous in engineering, naturally arising in applications such as PDE solving. Classical algorithms typically require $\mathcal{O}(N\sqrt{\kappa})$ time to solve a linear system, where κ is the condition number. The Harrow–Hassidim–Lloyd (HHL) algorithm, however, can achieve $\mathcal{O}(\text{poly}(\log(N\kappa^2)))$ time complexity (Harrow et al., 2009). Such quantum linear solvers have been proposed for accelerating large-scale FEM simulations in structural mechanics and materials modeling (Montanaro and Pallister, 2016; Clader et al., 2013), potentially reducing computation times in design and analysis phases of advanced manufacturing.

From the “solver” perspective, quantum computing has been explored in operations research for diverse optimization tasks. Quantum Approximate Optimization Algorithm (QAOA) and variational quantum eigensolvers have been applied to combinatorial scheduling problems, such as the Job-Shop Scheduling Problem (JSSP) (Farhi et al., 2014; Kurowski et al., 2023; Venturelli et al., 2016). In addition to scheduling, quantum algorithms have been investigated for quality control and defect detection in manufacturing. Quantum machine learning methods, such as quantum support vector machines (QSVM), have been applied to anomaly detection and defect classification in industrial manufacturing (Guijo et al., 2022), in some cases outperforming classical baselines in unbalanced datasets. Quantum-assisted anomaly detection has also been proposed for predictive maintenance of gas turbines in power plants (Sakhnenko et al., 2022). These studies illustrate that quantum computing has been shown to be effective in manufacturing. In the context of fuselage assembly, these quantum capabilities can potentially address two major challenges. First, quantum linear solvers offer the potential to accelerate FEM-based simulations, which dominate the cost of evaluating shape deviations, thereby enabling more rapid exploration of the design space. Second, quantum algorithms such as QAOA can improve the efficiency of determining optimal actuator forces by reducing the number of expensive simulation queries required. Together, these capabilities could greatly benefit actuator placement, enhance robustness to uncertainty, and support real-time quality control during aircraft assembly.

3 Quantum Bayesian Optimization for Fuselage Assembly

3.1 Preliminary

3.1.1 Bayesian Optimization

We first introduce vanilla BO. For a comprehensive introduction to BO, readers may refer to (Frazier, 2018; Garnett, 2023; Srinivas et al., 2009). BO is a powerful black-box optimization technique designed to efficiently identify optimal solutions to expensive-to-evaluate objective functions. Consider the following optimization problem:

$$y = f(x) + \xi,$$

where y represents the noisy observations with Gaussian noise ξ , and $f(\cdot)$ is an expensive-to-evaluate black-box function. The goal is to find the optimal solution x^* such that:

$$x^* = \arg \max_{x \in \mathcal{A}} f(x),$$

where \mathcal{A} denotes the feasible set. BO adopts a Sequential Model-Based Optimization (SMBO) framework, which primarily consists of two crucial components: (i) surrogate model, and (ii) optimization strategy.

The idea of the surrogate model is to model the response from the environment with respect to different inputs. The most common surrogate model within the BO framework is the Gaussian Process (GP). In GP, we assume that the objective function $f(x)$ follows a Gaussian Process such that: $f(x) \sim GP(m(x), K(x, x'))$, where $m(x)$ is the mean function and $K(x, x')$ is the covariance function. The mean function is the expectation of the objective function $m(x) = \mathbb{E}[f(x)]$. While the covariance function (kernel) describes the difference between outputs among different inputs $K(x, x') = \mathbb{E}[(f(x) - m(x))(f(x') - m(x'))]$. Several kernels can be employed, such as the linear kernel, Radial Basis Function (RBF) kernel, and Matérn kernel. In this paper, we adopt the RBF kernel: $K(\mathbf{x}, \mathbf{x}') = \exp\left(-\frac{\|\mathbf{x} - \mathbf{x}'\|^2}{2l^2}\right)$.

After modeling the response from the environment using GP, we can predict the output using the posterior of GP. Given historical observations $\mathcal{D}_t = \{\mathbf{X}_t, \mathbf{y}_t\}$, the posterior mean

and uncertainty at the new input x_* are expressed as:

$$\begin{aligned} m_t(x_*) &= K(x_*, \mathbf{X}_t) [K(\mathbf{X}_t, \mathbf{X}_t) + \sigma^2 \mathbf{I}]^{-1} \mathbf{y}_t \\ \sigma_t^2(x_*) &= K(x_*, x_*) - K(x_*, \mathbf{X}_t) [K(\mathbf{X}_t, \mathbf{X}_t) + \sigma^2 \mathbf{I}]^{-1} K(\mathbf{X}_t, x_*) \end{aligned} \quad (1)$$

For the optimization strategy, the essential step is selecting an appropriate acquisition function that balances exploration and exploitation when determining the next point to evaluate. In this paper, we utilize Upper Confidence Bound (UCB) as an acquisition function, defined in Eq. (2):

$$x_{optimal}^* = \arg \max_{x \in \mathcal{A}} m_t(x) + \beta \sigma_t(x), \quad (2)$$

where β controls the trade-off between exploration (favoring points with high uncertainty) and exploitation (favoring points with high predictive mean). Initially, when limited samples are available, UCB prioritizes exploration. As more data is collected, the algorithm increasingly exploits points with higher predicted means.

3.2 Problem Definition and Formulation

In aircraft assembly, shape deviations inevitably occur when two fuselage sections are joined due to shape mismatches. Composite materials used in aircraft construction have advantageous properties such as increased flexibility compared to traditional materials like metal and wood, making these fuselage sections easier to deform. Consequently, engineers need to carefully design the forces of actuators to precisely adjust the fuselage shapes, aligning them to reduce or eliminate the gap. In addition, measurement noise should also be considered during this process. To address these specific challenges, we adapted QBO to tackle this problem, a novel optimization method known for its sample efficiency. The primary input of our proposed QBO method is the combination of actuator forces that effectively minimizes the gap between fuselage sections during assembly.

In this problem, we follow the problem definition from the work (Lutz et al., 2024). We define n as the number of measurement points along the cross-section of the fuselage, with each point representing a position (x^i, y^i, z^i) . Additionally, m represents the number of actuators capable of applying forces along the fuselage edges over radial directions (Force denoted as $\mathbf{F} = (\mathbf{f}_1, \mathbf{f}_2, \dots, \mathbf{f}_n)$). When activated, these actuators either push or pull

to reshape the fuselage, guiding it from its initial shape towards a desired configuration. According to engineering constraints, actuator forces must remain within specified limits: $F_{min} \leq \mathbf{F}_i \leq F_{max}$. The initial shape is defined as the design shape, and its deformation is caused by gravity. Each measurement point of initial shape is defined as $\mathbf{P}_0^i = (x_0^i, y_0^i, z_0^i)$ for $i = 1, \dots, n$. The target shape and final shape denote the desired fuselage shape and the shape after applying actuators. Similar to each point of initial shape we defined previously, we denote $\mathbf{P}_t^i = (x_t^i, y_t^i, z_t^i)$ and $\mathbf{P}_f^i = (x_f^i, y_f^i, z_f^i)$ as the corresponding point of target shape the final shape. In practical manufacturing environments, measurement noise is unavoidable due to factors such as the dimensions of target objects and the accuracy of measurement equipment (Wang et al., 2023). The resulting deformation is characterized by the displacement vector $\mathbf{U} = (\mathbf{u}_1, \mathbf{u}_2, \dots, \mathbf{u}_n)$, which corresponds to the previously defined measurement points n . Displacements are directly influenced by the direction and magnitude of the applied forces and depend on the mechanical properties of the composite material used. The final shape can be expressed as adding the displacement vector to the initial shape, which is $\mathbf{P}_f = \mathbf{P}_0 + \mathbf{U} + \xi$, where ξ is measurement error. For each measurement point, the initial and final deviation $\vec{\delta}_0^i$ and $\vec{\delta}_f^i$ can be quantified as follows:

$$\begin{aligned}\vec{\delta}_0^i &= \mathbf{P}_t^i - \mathbf{P}_0^i \\ \vec{\delta}_f^i &= \mathbf{P}_t^i - \mathbf{P}_f^i = \vec{\delta}_0^i - \mathbf{u} + \xi\end{aligned}\tag{3}$$

Using Eq. (3), we define initial deviations and final deviations for all measurement points as $\Delta_0 = (\vec{\delta}_0^1, \vec{\delta}_0^2, \dots, \vec{\delta}_0^n)$ and $\Delta_f = (\vec{\delta}_f^1, \vec{\delta}_f^2, \dots, \vec{\delta}_f^n)$. These deviations effectively quantify the gaps in fuselage sections during assembly. In this problem, we apply mean absolute error (MAE) as our objective function to minimize:

$$\mathcal{L} = e_{MAE} = \frac{1}{N} \sum_i^N |\vec{\delta}_f^i|,\tag{4}$$

where N is the total number of measurement points. In order to formulate the problem of reducing the dimensional gap as a maximization problem, we add a negative sign in front of the mean absolute error, which is shown as follows.

$$\mathbf{F}^* = \arg \max -\mathcal{L}(\mathbf{F}) \quad s.t. \quad F_{min} \leq \mathbf{F} \leq F_{max}\tag{5}$$

In this paper, we specifically focus on developing a novel BO framework under quantum settings to efficiently solve the formulated optimization problem.

3.3 Methodology

3.3.1 Overview

Our proposed method mainly contains three modules: Quantum Oracle (QO) (Sec. 3.3.2), Mean Estimation (Sec. 3.3.3), and Weighted Bayesian Optimization (WBO) (Sec. 3.3.4). The first module is to build a quantum circuit that encodes possible shape deviations into a distribution. The second module is Mean Estimation, which retrieves the target shape deviations from the Quantum Oracle. Finally, the third module is similar to the acquisition function in classic BO, which guides the model to select the next promising input. In this section, we briefly introduce the ideas of quantum computing and its important concepts. Then, we introduce its weighted version and how we adapt it to the fuselage assembly. The pipeline of the proposed method is shown in Fig. 2.

3.3.2 Quantum Oracle

In this section, we use Dirac notation to introduce basic quantum computing preliminaries. The notation we used in this paper follows the notation used in (Sakurai and Napolitano, 2020). The quantum state is defined in Hilbert space, which has infinite dimensions. It can be represented as $|\alpha\rangle = \sum_{a'} c_{a'} |a'\rangle = \sum_{a'} |a'\rangle \langle a'|\alpha\rangle$, where $c_{a'} = \langle a'|\alpha\rangle$ is a complex coefficient. The probability of a' is defined as $|\langle a'|\alpha\rangle|^2$ for an arbitrary $|a'\rangle$ quantum state. In addition, Let us consider two quantum state systems, which is a composite system. Assuming that they are not entangled, we can write this quantum state as $|\psi\rangle_{A\otimes B} = |\phi\rangle_A \otimes |\phi\rangle_B$. We use \otimes to denote the tensor product. In quantum mechanics, the tensor product is to create the joint quantum state of multiple independent subsystems. For example, a two-level system can be denoted as $|\Psi\rangle_{1\otimes 2} = |1\rangle_1 \otimes \frac{1}{\sqrt{2}}(|1\rangle_2 + |0\rangle_2)$.

Quantum computing is executed by the quantum circuits. Similar to classic computers, there are logic gates in quantum computers, which transfer and operate a qubit to realize a computational purpose. Mathematically, every quantum gate is a unitary operator, so that the quantum state can evolve to another state. For example, consider a quantum gate called the Hadamard gate:

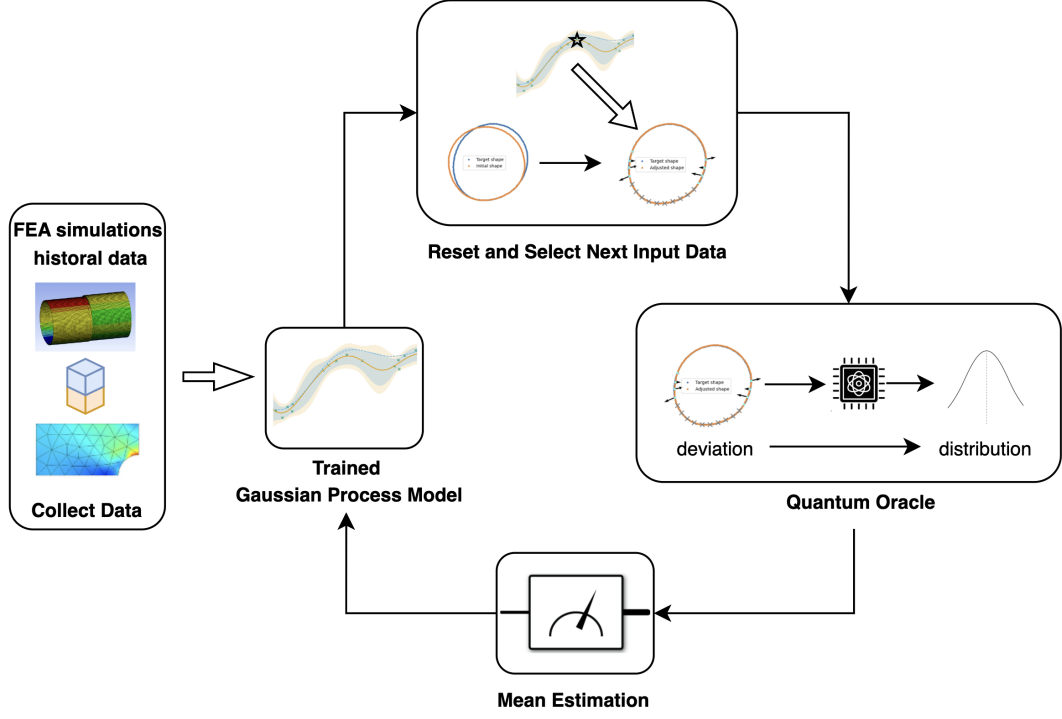


Figure 2: The pipeline of our proposed method. Data from FEA simulations are first collected and used to train a Gaussian Process surrogate model. Based on the GP posterior, the acquisition function selects the next force combinations. The quantum oracle encodes deviations into a distribution, and mean estimation evaluates the candidate force combinations through repeated queries. The new observation and candidate force combinations update the GP posterior.

$$H = \frac{1}{\sqrt{2}} \begin{bmatrix} 1 & 1 \\ 1 & -1 \end{bmatrix},$$

then we apply the gate to a single qubit system, $|0\rangle = (1, 0)^T$, i.e. $H|0\rangle = \frac{1}{\sqrt{2}}(1, 1)^T = \frac{1}{\sqrt{2}}(|0\rangle + |1\rangle)$. Hence, the original quantum state $|0\rangle$ evolves into another quantum state $\frac{1}{\sqrt{2}}(|0\rangle + |1\rangle)$.

Quantum oracle encodes possible values of a distribution. Mathematically, in this paper, we define the quantum oracle as a unitary operator that encodes the reward distribution, as shown in Eq. (6) (Dai et al., 2023).

$$\mathcal{O} : |0\rangle \rightarrow \sum_{\omega \in \Omega} \sqrt{P(\omega)} |\omega\rangle |y(\omega)\rangle, \quad (6)$$

where $|\omega\rangle$ is possible states, $\sqrt{P(\omega)}$ probability amplitude of the state $|\omega\rangle$ and $|y(\omega)\rangle$ is the reward corresponding to $|\omega\rangle$. In the case of fuselage assembly, $|\omega\rangle$ denotes as different final shapes, $|y(\omega)\rangle$ denotes as observations (i.e., deviation), and $P(\omega)$ is the probability that state $|\omega\rangle$ appears.

3.3.3 Mean Estimation

Mean estimation refers to methods employed to extract response values from a quantum oracle. In this paper, we utilize the *quantum Monte Carlo* (QMC) algorithm. Leveraging quantum methods allows for fewer samples to achieve the same estimation accuracy compared to classical algorithms

Lemma 1. (Quantum Monte Carlo method (Montanaro, 2015)) *Assume that $y : \Omega \rightarrow \mathbb{R}$ is a random variable with bounded variance, Ω is equipped with a probability measure P , and the quantum unitary oracle \mathcal{O} encodes P and y .*

- *If $y \in [0, 1]$, there is a constant $C_1 > 1$ and a quantum algorithm $QMC_1(\mathcal{O}, \epsilon, \delta)$ which returns an estimate \hat{y} of $\mathbb{E}[y]$ such that $\Pr(|\hat{y} - \mathbb{E}[y]| \geq \epsilon) \leq \delta$ using at most $\frac{C_1}{\epsilon} \log \frac{1}{\delta}$ queries to \mathcal{O} and \mathcal{O}^\dagger .*
- *If y has bounded variance, i.e., $\text{Var}(y) \leq \sigma^2$, then for $\epsilon < 4\sigma$, there is a constant $C_2 > 1$ and a quantum algorithm $QMC_2(\mathcal{O}, \epsilon, \delta)$ which returns an estimate \hat{y} of $\mathbb{E}[y]$ such that $\Pr(|\hat{y} - \mathbb{E}[y]| \geq \epsilon) \leq \delta$ using at most*

$$\frac{C_2 \sigma}{\epsilon} \log_2^{3/2} \left(\frac{8\sigma}{\epsilon} \right) \log_2 \left(\log_2 \frac{8\sigma}{\epsilon} \right) \log \frac{1}{\delta}$$

queries to \mathcal{O} and \mathcal{O}^\dagger .

In classic mean estimation settings, consider Chebyshev's inequality:

$$\mathbb{P}(|\hat{\mu} - \mu| \geq \epsilon) \leq \frac{\sigma^2}{k\epsilon^2},$$

where ϵ denotes the desired accuracy, σ the variance, and k the number of samples. We can infer that achieving an error bound ϵ requires $k = O(\sigma^2/\epsilon^2)$ samples (queries). However,

the quantum algorithms significantly reduce this complexity to $O(1/\epsilon)$ samples (queries) to reach the same accuracy. In the case of fuselage assembly, suppose the measurement noise is $\sigma = 0.1$, the error bound is $\epsilon = 0.01$, and the confidence level is $1 - \delta = 0.95$. Chebyshev’s bound yields $k \geq 2,000$ samples in the classical setting, whereas a quantum algorithm can achieve comparable accuracy with roughly 1,266 oracle queries (depending on the choices of C_2).

3.3.4 Algorithm

In this section, we adapt the frameworks in QBO and WBO (Dai et al., 2023; Deng et al., 2022) to fuselage assembly tasks in manufacturing. Consistent with QBO (Dai et al., 2023), we adopt the same notation in that work. The complete algorithm is summarized in Algorithm 1.

Algorithm 1 QBO for Fuselage Assembly

Require: Gaussian Process with hyperparameter l , total queries T , regularization λ , confidence ellipse β , trade-off parameter η , and successful rate δ .

- 1: Randomly pick a force combination $\mathbf{F} \in \mathcal{A}$
 - 2: **for** stage $s = 1, 2, \dots$ (Stop algorithm when T queries are used) **do**
 - 3: $\mathbf{F}_s = \arg \max_{\mathbf{F} \in \mathcal{A}} \tilde{\mu}_{s-1}(\mathbf{F}) + \beta_s \tilde{\sigma}_{s-1}(\mathbf{F})$
 - 4: $\epsilon_s = \tilde{\sigma} / \sqrt{\lambda}$
 - 5: **while** $\sum_{k=1}^s N_\epsilon \leq T$ **do**
 - 6: Run QMC($\mathcal{O}, \eta \epsilon_s, \delta$) to query the shape deviation y_s
 - 7: **end while**
 - 8: Update the GP posterior using known data pairs $(\mathbf{F}_s, \mathbf{y}_s)$
 - 9: **end for**
-

Initially, we assume that the surrogate model is a function $f : \mathcal{X} \rightarrow \mathbb{R}$, where $\mathcal{X} \subseteq \mathbb{R}^d$. The function f is assumed to sample from a Reproducing Kernel Hilbert Space (RKHS), associated with a kernel function K . The induced RKHS norm satisfies $\|f\|_k = \sqrt{\langle f, f \rangle_k} \leq \infty$. There are many choices of surrogate models in BO, such as the weighted Gaussian Process (Deng et al., 2022), the parametric function (Siam et al., 2025), and the deep uncertainty model (Chen et al., 2024). In this work, we adopt Weighted Gaussian Process

(WGP) as the surrogate model. Relative to a standard Gaussian Process, the WGP provides better modeling capacity while preserving the advantage of having explicit mathematical formulations like the standard Gaussian Process.

We then define the cumulative regret in Eq. (7)

$$R_T = \sum_{i=1}^T (f(x_*) - f(x_i)), \quad (7)$$

where T means the number of samples. Theoretically, the cumulative regret upper bound of QBO can be achieved $\mathcal{O}(\text{poly log } T)$ (Dai et al., 2023), which breaks the lower bound of the classic algorithm $\Omega(\sqrt{T})$ (ignoring log factors) (Scarlett et al., 2017).

Lemma 2. (QBO Cumulative Regret Upper Bound (Dai et al., 2023)) *With probability of at least $1 - \delta$, we have that*

$$\begin{aligned} R_T &= \mathcal{O}\left(d^{3/2}(\log T)^{3/2} \log(d \log T)\right), \quad \text{linear kernel,} \\ R_T &= \mathcal{O}\left((\log T)^{3(d+1)/2} \log((\log T)^{d+1})\right), \quad \text{exponential (SE) kernel.} \end{aligned}$$

In Step 3, at each stage s , the acquisition function guides the model to select promising inputs based on a linear combination of posterior mean and uncertainty. In this paper, we use a weighted posterior mean and uncertainty, which is different from that in the previous section 3.1.1. We define the weighted matrix as $W_s = \text{diag}(1/\sigma_1^2, \dots, 1/\sigma_s^2)$, a diagonal matrix of size $s \times s$. The weighted matrix is the core part of the weighted posterior mean and uncertainty. Intuitively, this weighted scheme assigns higher significance to existing samples with lower uncertainty when predicting the responses of new inputs.

Using the weighted matrix, we redefine quantities from the previous section into their weighted version:

$$\begin{aligned} \tilde{K}(\mathbf{X}_t, \mathbf{X}_t) &= W_s^{1/2} K(\mathbf{X}_t, \mathbf{X}_t) W_s^{1/2} \\ \tilde{K}(x_*, \mathbf{X}_t) &= \tilde{K}^T(\mathbf{X}_t, x_*) = W_s^{1/2} K(x_*, \mathbf{X}_t) \\ \tilde{\mathbf{y}}_t &= W_s^{1/2} \mathbf{y}_t \end{aligned}$$

With these weighted definitions, the posterior distribution from Eq. (1) is updated as:

$$\begin{aligned} \tilde{m}_t(x_*) &= \tilde{K}(x_*, \mathbf{X}_t) \left[\tilde{K}(\mathbf{X}_t, \mathbf{X}_t) + \lambda \mathbf{I} \right]^{-1} \tilde{\mathbf{y}}_t \\ \tilde{\sigma}_t^2(x_*) &= K(x_*, x_*) - \tilde{K}(x_*, \mathbf{X}_t) \left[\tilde{K}(\mathbf{X}_t, \mathbf{X}_t) + \lambda \mathbf{I} \right]^{-1} \tilde{K}(\mathbf{X}_t, x_*), \end{aligned} \quad (8)$$

where λ is the regularization parameter. The size of \tilde{K} in Eq. (8) increases with queries. If the algorithm requires at least T queries to terminate, the time complexity of the calculation of the inversion matrix $(\tilde{K} + \lambda \mathbf{I})^{-1}$ is $\mathcal{O}(T^3)$, which is time-consuming when T is sufficiently large. Hence, to solve this problem, we use an alternative way to update posterior mean and uncertainty, as shown in Eq. (9), which is mathematically equivalent to Eq. (8). The full proof is in Appendix A from the work (Dai et al., 2023).

$$\begin{aligned}\tilde{m}_t(x_*) &= \tilde{K}(x_*, \mathbf{X}_t) \left[\tilde{K}(\mathbf{X}_t, \mathbf{X}_t) + \lambda \mathbf{I} \right]^{-1} \tilde{\mathbf{y}}_t = \phi(x_*)^\top V_t^{-1} \Phi_t^\top W_t \mathbf{y}_t \\ \tilde{\sigma}_t^2(x_*) &= K(x_*, x_*) - \tilde{K}(x_*, \mathbf{X}_t) \left[\tilde{K}(\mathbf{X}_t, \mathbf{X}_t) + \lambda \mathbf{I} \right]^{-1} \tilde{K}(\mathbf{X}_t, x_*) \\ &= \lambda \phi(x_*)^\top V_t^{-1} \phi(x_*),\end{aligned}\tag{9}$$

where ϕ and Φ are feature mappings.

In this paper, it is worth noting that we adopt random Fourier features (RFF) to approximate the kernel function, such that $K(x, x') \approx \phi^T(x)\phi(x')$. Rahimi and Recht (2007) proposed an approximation using low-dimensional features of the kernel function. The key idea of approximation is that we can find a map such that $\mathbb{R}^D \mapsto \mathbb{R}^R$, where $R \ll T$. Here, we adapt Bochner’s theorem from the work (Rahimi and Recht, 2007).

Bochner’s theorem (Rudin, 2017) *A continuous kernel $k(x, y) = k(x - y)$ on \mathbb{R}^d is positive definite if and only if $k(\delta)$ is the Fourier transform of a non-negative measure.*

From Bochner’s theorem, we can construct the kernel function as follows:

$$k(x, y) = k(x - y) = \int_{\mathbb{R}^R} p(\omega) e^{j\omega'(\mathbf{x}-\mathbf{y})} d\omega = \mathbb{E}_\omega[\zeta_\omega(\mathbf{x})\zeta_\omega(\mathbf{y})^*],$$

where $\zeta_\omega(\mathbf{x}) = e^{j\omega'\mathbf{x}}$. By adopting Bochner’s theorem, we can construct RFF to approximate RBF kernel. The proof is shown in Appendix A. The number of RFF (R) is set as 1024.

In Steps 5 and 6, setting the precision ϵ_s , trade-off parameter η , and the confidence level δ , we utilize the QMC algorithm to evaluate the mean of the selected force combinations from the acquisition function. This step introduces the major improvement in sample efficiency in our framework. As shown in Lemma 1 (Sec. 3.3.3), QMC requires fewer queries than classical Monte Carlo methods to achieve the same precision and confidence level, thereby reducing evaluation costs in noisy manufacturing environments. The trade-off parameter η is introduced in work (Hikima et al., 2024), which controls estimation

accuracy. Specifically, it balances the maximum stages s_{max} and regret incurred in each stage s . Intuitively, more stages come with a larger η . Hence, each stage has a larger regret than the stage with a smaller η .

4 Experiments

4.1 Overview

In the case study, our experiments are conducted using a simulated environment for fuselage assembly (Lutz et al., 2024). Specifically, we simulate the joining of two fuselage sections, where one section remains stationary. The other section is manipulated by a series of equally spaced, force-controlled actuators placed along its edge. These actuators can apply pushing or pulling forces to adjust the fuselage position, aiming to minimize the assembly gap between the two sections.

The optimization objective involves identifying the optimal directions and magnitudes of forces exerted by these actuators. To closely replicate realistic manufacturing conditions, we incorporate measurement noise into our experimental setup. We introduce a Gaussian noise ξ to each measurement point. In the results section, we present a comparative analysis of sample efficiency between classical BO and QBO.

4.2 Experiment Settings

4.2.1 Environment

In our fuselage assembly scenario, the experimental environment can be established through two approaches: (i) ANSYS Design Language (pyMAPDL) (Kaszynski, 2021), and (ii) surrogate modeling. The ANSYS environment utilizes the finite element method (FEM) (Szabó and Babuška, 2021) to determine the fuselage’s displacement response to various proposed force pairs. It should be pointed out that these displacement computations rely heavily on finite element analysis (FEA), which can be computationally demanding and time-consuming. However, recent advancements in materials science have indicated that the relationship between applied forces and displacement can be effectively approximated using a linear model, significantly simplifying and accelerating calculations (Dowling, 2007).

Du et al. (2019) proposed a linear surrogate model to approximate the displacement:

$$Y_i = F_D \cdot \mathbf{U} + \epsilon,$$

where Y_i represents the displacement, F_D denotes the design forces from experimental designs, and ϵ is noise. Consequently, the displacement matrix \mathbf{U} can be obtained by regression analysis using known displacement and force data. In this paper, we adopt this surrogate model as our computational environment.

Regarding the action and observation spaces, our experiments follow a similar approach to the work (Lutz et al., 2024). Specifically, we select 8 candidate positions to install force-controlled actuators for shape adjustment. Each actuator has a defined force range constrained to $F_i \in [-500, 500]$ (lb). Here, a negative force value indicates that the direction of the force is oriented inward, towards the fuselage interior.

On the other hand, our observation space captures the fuselage’s deviation from its original geometry under the influence of these applied forces. We select $N = 177$ measurement nodes positioned on the fuselage to evaluate these deviations, with each node corresponding to an (x, y) coordinate. From these nodes, we define two key quantities: (i) the initial shape deviation Δ_{MAE}^0 , and (ii) the final shape deviation Δ_{MAE}^f (dimensional gap).

With these elements defined, we can construct the observation array \mathbf{y} . To align with the Mean Estimation framework described in Sec. 3.3.3, we modify the reward function originally presented in Eq. (4). Specifically, we use the ratio of current dimensional error with initial error, as formulated in Eq. (10).

$$\mathcal{L}_{scale} = -\frac{e_{MAE}^f}{e_{MAE}^0} \quad (10)$$

Hence, the problem is transferred from minimizing the gap to maximizing the \mathcal{L}_{scale} , i.e.

$$\mathbf{F}^* = \arg \max \mathcal{L}_{scale}(\mathbf{F}) \quad s.t. \quad -500 \leq \mathbf{F} \leq 500$$

In the classical setting, we determine the number of required queries using Chebyshev’s inequality, such that $n = \left\lceil \frac{\sigma^2}{\epsilon^2 \delta} \right\rceil$, where δ is the confidence level, ϵ is the accuracy, and σ is the standard deviation.

4.3 Result

In this section, we compare cumulative regrets between classical BO and QBO under two different noise levels. In Wang et al. (2023), the noise sources in manufacturing come from two factors: (i) the overall scale of the target object and (ii) the accuracy of the metrology tool. In our fuselage case, the Laser Distance Meter (LDM) has a minimum measurement error of approximately 0.08 in + 0.004 in/m (≈ 2 mm + 0.1 mm/m). Considering these contributors for a fuselage with a characteristic dimension of 5 m, the absolute error is about 0.1 in. Hence, we evaluate two observation-noise levels, $\sigma \in \{0.1, 0.2\}$, which are reasonable for our experiment setup.

In classical BO, we adopt the design following the MINI-META framework (Calandriello et al., 2022) to facilitate mean estimation for the noisy observation. Calandriello et al. (2022) introduced a meta-algorithm that encourages repeated sampling of the same candidate rather than changing often. The work shows that this algorithm maintains the same regret rate as the traditional BO algorithm (Srinivas et al., 2009). Particularly, we add a Monte Carlo estimation module to estimate the mean of observations given the precision ϵ_s and confidence level δ .

4.3.1 Discrete Cases

In this subsection, we consider a case in which only two actuators are assigned active forces, while the remaining actuators are fixed at zero, as shown in Fig. 3. The feasible force range is discretized into $\mathcal{A} = 21$ uniformly spaced values within $[-500, 500]$ lbs. Consequently, the total number of possible force combinations for the two actuators is $21^2 = 441$, and the minimum mean absolute error (MAE) among these 441 combinations is 0.048 in. Fig. 4(a) presents the cumulative regret curves of QBO and classic BO for a specific initial deviation. The curves corresponding to the quantum setting converge around 2,000 iterations, whereas those for the classical setting continue to increase. Moreover, the upper bound of cumulative regret achieved by the quantum algorithm is consistently lower than that of its classical algorithm. Fig. 4(b) further examines running-minimum MAE versus iteration under two noise levels. In the figure, the vertical dashed line at 2,000 iterations marks that QBO reaches the optimal points within 2,000 iterations, which corresponds to the previous

conclusion. However, classic BO cannot find the optimal solutions in 3,000 iterations under both noise levels. The results highlight the sample-efficiency advantages of the QBO over classic BO.

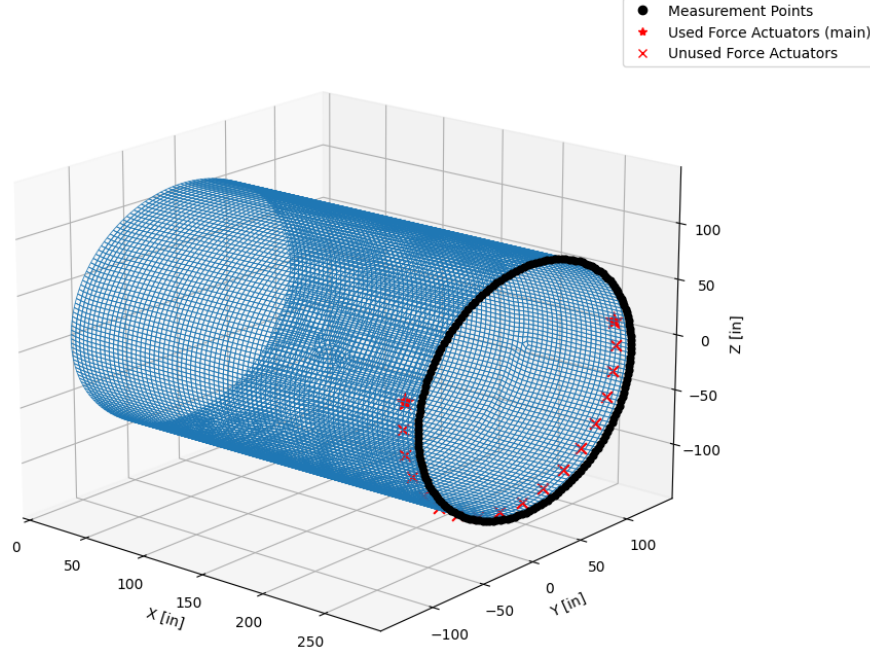


Figure 3: Scheme of 2 actuators used in the fuselage shape control.

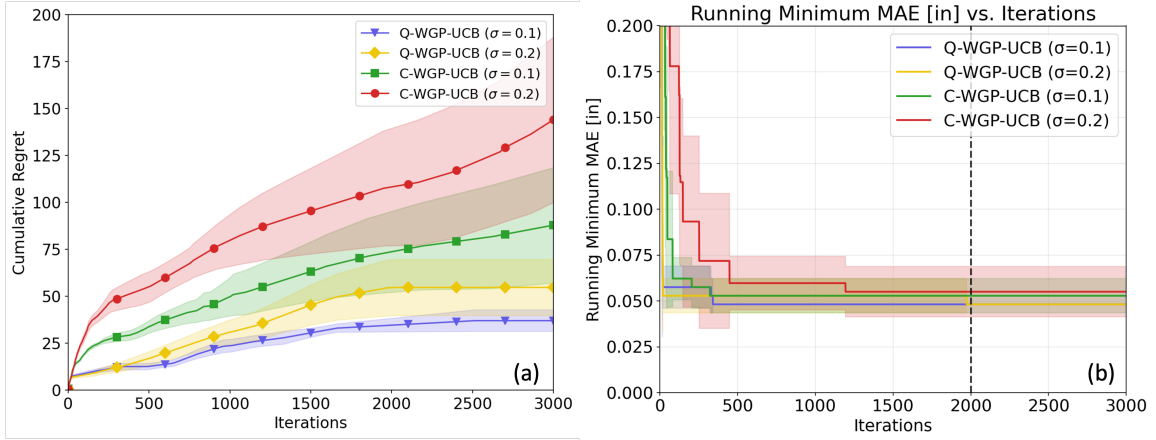


Figure 4: (a) Comparison of cumulative regrets between classic BO and QBO in discrete cases. (b) Compare the best shape control performance between classic BO and QBO with 2 actuators. The black dashed line marks the incumbent after 2,000 iterations.

4.3.2 Continuous Cases

In this subsection, we examine the cases with 8 actuators with a continuous force range. As shown in Fig. 5(a), the cumulative regret for QBO becomes stable after approximately 400 iterations for both noise levels. This indicates that the algorithm successfully finds some desired actuator force combinations that lead to near-zero dimensional mismatches. Although the confidence interval of QBO is larger than that of classic BO on both noise levels, QBO has a larger search spectrum and thus finds more different optimal solutions. Conversely, the cumulative regrets of the classical BO algorithm continue to rise, highlighting that the model still explores the optimal solution. Although the confidence intervals of QBO are broader than those of classic BO at both noise levels, QBO explores a wider search space and thus discovers a greater diversity of optimal solutions. Moreover, Fig. 5(b) compares the minimum MAE achieved by QBO and classic BO under two noise levels. The results clearly demonstrate the superior sample efficiency of the quantum algorithm. The Q-GP-UCB curves rapidly decrease within the first 2,500 iterations and then stabilize, indicating that the quantum algorithm reaches high-quality solutions using significantly fewer iterations. In contrast, classic BO requires more iterations to achieve comparable performance, and their convergence is slower.

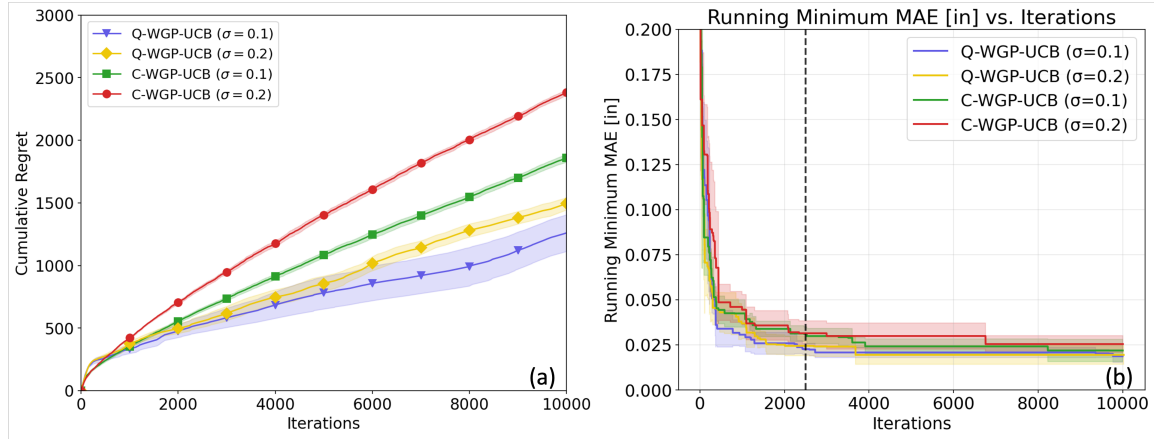


Figure 5: (a) Comparison of Cumulative regrets between classic BO and QBO using 8 actuators in fuselage assembly. (b) Compare the best shape control performance between classic BO and QBO with 8 actuators. The black dashed line marks the incumbent after 2,500 iterations.

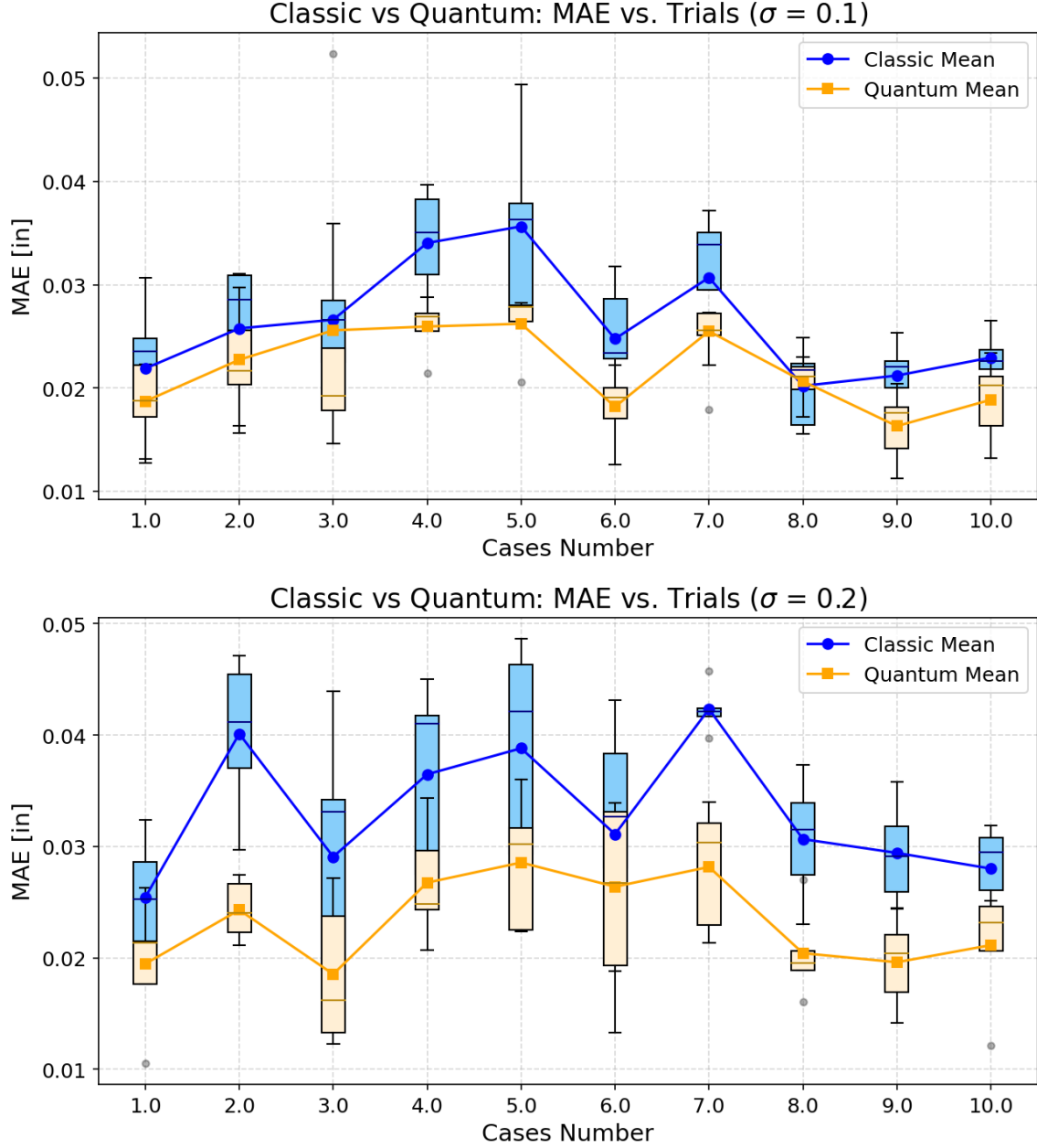


Figure 6: Experiments on 10 test initial conditions under $\sigma = 0.1$ using QBO (orange) and classic BO (blue). We run 5 times for every initial shape for all experiments.

To further evaluate the robustness and generalizability of our proposed method, we perform 10 distinct initial conditions between QBO and classic BO. We run 5 experiments for each trial. Fig. 6 provides box plots that summarize the MAE across 10 experimental

trials. Each box plot illustrates the interquartile range (IQR), bounded by the first quartile (Q1) and third quartile (Q3), with the median MAE highlighted by a horizontal orange line. Furthermore, we report the mean MAE and standard deviation of MAE from the experiment with the smallest MAE across 10 trials. Generally, QBO has better performance than classic BO with lower MAE in all experiment trials (either with lower mean MAE or low standard deviation).

	$\sigma = 0.1$	$\sigma = 0.2$
QBO	0.022 ± 0.004	0.023 ± 0.004
Classic BO	0.026 ± 0.005	0.033 ± 0.006

Table 1: Mean of MAE and corresponding standard deviation of 5 runs (small is better) across 10 experimental trials between QBO and classic BO.

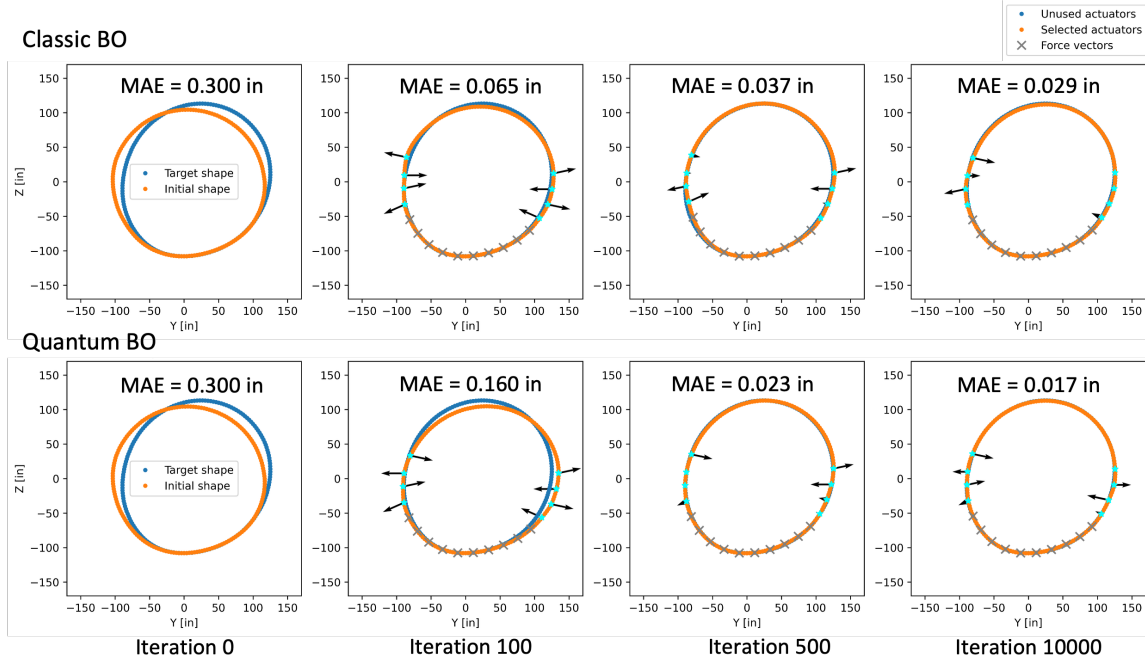


Figure 7: Shape adjustment results (cross section) using QBO (bottom) and classic BO (top) at noise level $\sigma = 0.1$. The length of each force vector represents the magnitude of the applied force. Both scenarios use the same initial condition. The best shape control results received by classic BO and QBO at iterations 100, 500, and 10,000 are demonstrated, respectively.

Instead of only demonstrating the final optimization results, we uncover the intermediate optimization results received by classic BO and QBO in Fig. 7, in which the best shape control results received after 100, 500, and 10000 iterations are demonstrated. The initial condition is sampled from 10 test initial conditions. The placement of these actuators facilitates horizontal adjustments rather than vertical ones. To show accuracy and reliability, MAE is computed using ANSYS software (FEA-based method) rather than a surrogate model. Initially, the MAE for shape mismatch is measured at 0.3 for one specific initial condition. After shape control, the dimensional mismatches are significantly reduced to 0.029 and 0.017 under noise levels of $\sigma = 0.1$, respectively, demonstrating the effectiveness of our method. It is worth noting that at the first 100th iteration, the classic BO achieves a lower MAE than the quantum BO. This result aligns with the cumulative regret curve, shown in Fig. 5, where the cumulative regret of QBO is higher in the early iterations. This behavior indicates that QBO is actively exploring a wider range of solutions, trying different combinations of actuator force before converging. In addition, we can also find out that the optimization results received by QBO with 500 iterations are even better than the results received by the classic BO with 10000 iterations, which further demonstrates the sample efficiency of QBO.

5 Conclusion

In this paper, we propose a Quantum Bayesian Optimization framework for optimal actuator placement of the fuselage assembly. In aircraft manufacturing, fuselage sections are built separately and later joined, potentially leading to dimensional mismatches between sections that compromise aircraft safety. To reduce catastrophic risks, precise shape control through force-controlled actuator placement is essential. However, accurately determining the optimal set of actuator forces has several challenges: (i) the continuous nature of actuator forces yields infinite potential solutions, and (ii) evaluating the resulting shape deviation for each candidate force combination is computationally intensive.

To address these limitations, we proposed QBO, which leverages quantum computing to significantly reduce the number of required samples compared to its classical optimization algorithms, particularly under noisy conditions. Through simulated experiments, we

demonstrated that our quantum-based method achieves tighter cumulative regrets under two noisy conditions, demonstrating its sample efficiency in finding optimal actuator forces. Further, the FEA-based evaluations show that our proposed method successfully adjusts shape mismatches. Additionally, we performed our algorithm on 10 different initial conditions and confirmed that our method consistently delivers statistically stable MAE at two noise levels, which shows its practical reliability.

Although our proposed method achieves promising results, there is some room for improvement. Notably, the current QBO does not account for complex physical constraints when searching over the force pairs. In actual shape control, the residual stress is an important factor to be considered. High residual stress can induce structural failure and affect overall fuselage integrity. Specifically, Tsai-Wu failure criterion, which is a widely used material failure theory for composite material, needs to be satisfied when applied forces. Without incorporating these constraints into the optimization process, the proposed force pairs could result in non-feasible solutions in reality. The future work will develop a constrained quantum acquisition function that ensures the optimization respects the feasible ranges of residual stress, preventing the solutions that could result in impracticality in the real assembly process. In addition to incorporating the Tsai–Wu failure criterion into the optimization process, another important direction is to transfer the current simulator-based quantum optimization framework to a real quantum computer. While all experiments in this study were performed on classical simulators, the ultimate goal is to deploy the proposed QBO framework on actual quantum processors, such as IBM Quantum or other NISQ devices.

A Proof of Approximation RBF Kernel

Suppose $\omega \sim N(0, 1)$, and $p(\omega)$ is a probability density function.

$$\begin{aligned}\mathbb{E}_\omega(\zeta_\omega(\mathbf{x})\zeta_\omega(\mathbf{y})^*) &= \mathbb{E}_w(\exp(j\omega\mathbf{x})\exp(-j\omega\mathbf{y})) = \mathbb{E}_w(\exp(jw(\mathbf{x} - \mathbf{y}))) \\ &= \int_{\mathbb{R}^R} p(\omega)\exp(j\omega(\mathbf{x} - \mathbf{y})) d\omega = \int_{\mathbb{R}^R} \exp(-\frac{1}{2}\omega^2)\exp(jw(\mathbf{x} - \mathbf{y}))d\omega \\ &= (\sqrt{2\pi})^{-R} \int_{\mathbb{R}^R} \exp(-\frac{1}{2}(\omega^2 - 2jw\delta - \delta^2) - \frac{1}{2}\delta^2)d\omega, \quad \text{where } \delta = \mathbf{x} - \mathbf{y} \\ &= (\sqrt{2\pi})^{-R} \exp(-\frac{1}{2}\delta^2) \int_{\mathbb{R}^R} \exp(-\frac{1}{2}(\omega - j\delta)^2)d\omega \\ &= (\sqrt{2\pi})^{-R} \cdot (\sqrt{2\pi})^R \exp(-\frac{1}{2}(\mathbf{x} - \mathbf{y})^2) \\ &= \exp(-\frac{1}{2}(\mathbf{x} - \mathbf{y})^2).\end{aligned}$$

Data Availability Statement

The data supporting the findings of this study will be made available from the corresponding author upon reasonable request after the publication of this paper.

References

- AlBahar, A., I. Kim, T. Lutz, and X. Yue (2022). Stress-aware optimal placement of actuators for ultra-high precision quality control of composite structures assembly. In *2022 IEEE 18th International Conference on Automation Science and Engineering (CASE)*, pp. 2178–2183. IEEE.
- AlBahar, A., I. Kim, X. Wang, and X. Yue (2023). Physics-constrained bayesian optimization for optimal actuators placement in composite structures assembly. *IEEE Transactions on Automation Science and Engineering* 20(4), 2772–2783.
- Calandriello, D., L. Carratino, A. Lazaric, M. Valko, and L. Rosasco (2022). Scaling gaussian process optimization by evaluating a few unique candidates multiple times. In *International Conference on Machine Learning*, pp. 2523–2541. PMLR.
- Chen, J., P. Ou, Y. Chang, H. Zhang, X.-Y. Li, E. H. Sargent, and W. Chen (2024). Adaptive catalyst discovery using multicriteria bayesian optimization with representation learning. *arXiv preprint arXiv:2404.12445*.
- Clader, B. D., B. C. Jacobs, and C. R. Sprouse (2013). Preconditioned quantum linear system algorithm. *Physical review letters* 110(25), 250504.
- Dai, Z., G. K. R. Lau, A. Verma, Y. Shu, B. K. H. Low, and P. Jaillet (2023). Quantum bayesian optimization. *Advances in Neural Information Processing Systems* 36, 20179–20207.

- Deng, Y., X. Zhou, B. Kim, A. Tewari, A. Gupta, and N. Shroff (2022). Weighted gaussian process bandits for non-stationary environments. In *International Conference on Artificial Intelligence and Statistics*, pp. 6909–6932. PMLR.
- Dowling, N. E. (2007). Engineering methods for deformation, fracture and fatigue. *Mechanical behavior of materials*, 152–154.
- Du, J., S. Cao, J. H. Hunt, X. Huo, and J. Shi (2022, July). A new sparse-learning model for maximum gap reduction of composite fuselage assembly. *Technometrics* 64(3), 409–418.
- Du, J., X. Yue, J. H. Hunt, and J. Shi (2019, October). Optimal placement of actuators via sparse learning for composite fuselage shape control. *Journal of Manufacturing Science and Engineering* 141(10), 101004.
- Farhi, E., J. Goldstone, and S. Gutmann (2014). A quantum approximate optimization algorithm. *arXiv preprint arXiv:1411.4028*.
- Frazier, P. I. (2018). Bayesian optimization. In *Recent advances in optimization and modeling of contemporary problems*, pp. 255–278. Informa.
- Garnett, R. (2023). *Bayesian optimization*. Cambridge University Press.
- Guijo, D., V. Onofre, G. Del Bimbo, S. Mugel, D. Estepa, X. De Carlos, A. Adell, A. Lojo, J. Bilbao, and R. Orus (2022). Quantum artificial vision for defect detection in manufacturing. *arXiv preprint arXiv:2208.04988*.
- Harrow, A. W., A. Hassidim, and S. Lloyd (2009). Quantum algorithm for linear systems of equations. *Physical review letters* 103(15), 150502.
- Hikima, Y., K. Murao, S. Takemori, and Y. Umeda (2024). Quantum kernelized bandits. In *The 40th Conference on Uncertainty in Artificial Intelligence*.
- Kaszynski, A. (2021, November). pyansys: Pythonic interface to MAPDL.
- Kurowski, K., T. Pecyna, M. Slys, R. Rozycki, G. Waligora, and J. Weglarz (2023). Application of quantum approximate optimization algorithm to job shop scheduling problem. *European Journal of Operational Research* 310(2), 518–528.
- Lutz, T., Y. Wang, X. Yue, and J. C. and (2024). Reinforcement learning for fuselage shape control during aircraft assembly. *IISE Transactions* 0(0), 1–15.
- Montanaro, A. (2015). Quantum speedup of monte carlo methods. *Proceedings of the Royal Society A: Mathematical, Physical and Engineering Sciences* 471(2181), 20150301.
- Montanaro, A. and S. Pallister (2016). Quantum algorithms and the finite element method. *Physical Review A* 93(3), 032324.
- Mou, S., M. Biehler, X. Yue, J. H. Hunt, and J. S. and (2023). Spac: Sparse sensor placement-based adaptive control for high precision fuselage assembly. *IISE Transactions* 55(11), 1133–1143.
- Rahimi, A. and B. Recht (2007). Random features for large-scale kernel machines. *Advances in neural information processing systems* 20.

- Rudin, W. (2017). *Fourier analysis on groups*. Courier Dover Publications.
- Sakhnenko, A., C. O’Meara, K. J. Ghosh, C. B. Mendl, G. Cortiana, and J. Bernabé-Moreno (2022). Hybrid classical-quantum autoencoder for anomaly detection. *Quantum Machine Intelligence* 4(2), 27.
- Sakurai, J. J. and J. Napolitano (2020). *Modern quantum mechanics*. Cambridge University Press.
- Scarlett, J., I. Bogunovic, and V. Cevher (2017). Lower bounds on regret for noisy gaussian process bandit optimization. In *Conference on Learning Theory*, pp. 1723–1742. PMLR.
- Siam, Z. S., C. Guan, and C. Liu (2025). Quantum non-linear bandit optimization. *arXiv preprint arXiv:2503.03023*.
- Srinivas, N., A. Krause, S. M. Kakade, and M. Seeger (2009). Gaussian process optimization in the bandit setting: No regret and experimental design. *arXiv preprint arXiv:0912.3995*.
- Szabó, B. and I. Babuška (2021). Finite element analysis: Method, verification and validation.
- Venturelli, D., D. Marchand, and G. Rojo (2016). Job shop scheduling solver based on quantum annealing. In *Proc. of ICAPS-16 Workshop on Constraint Satisfaction Techniques for Planning and Scheduling (COPLAS)*, pp. 25–34.
- Wang, Y., T. Lutz, X. Yue, and J. Du (2024). Smartfixture: Physics-guided reinforcement learning for automatic fixture layout design in manufacturing systems. *IISE Transactions*, 1–16.
- Wang, Y., W. Sun, J. Jin, Z. Kong, and X. Yue (2023). Mvgcn: Multi-view graph convolutional neural network for surface defect identification using three-dimensional point cloud. *Journal of Manufacturing Science and Engineering* 145(3), 031004.
- Wang, Y. and X. Yue (2012). Multimodal deep learning for manufacturing systems: Recent progress and future trends. *Multimodal and Tensor Data Analytics for Industrial Systems Improvement*, 221–252.
- Wen, Y., X. Yue, J. H. Hunt, and J. Shi (2018). Feasibility analysis of composite fuselage shape control via finite element analysis. *Journal of Manufacturing Systems* 46, 272–281.
- Wen, Y., X. Yue, J. H. Hunt, and J. Shi (2019). Virtual assembly and residual stress analysis for the composite fuselage assembly process. *Journal of Manufacturing Systems* 52, 55–62.
- Yue, X., Y. Wen, J. H. Hunt, and J. Shi (2018, 02). Surrogate model-based control considering uncertainties for composite fuselage assembly. *Journal of Manufacturing Science and Engineering* 140(4), 041017.
- Zhong, Z., S. Mou, J. H. Hunt, and J. Shi (2022, 02). Finite element analysis model-based cautious automatic optimal shape control for fuselage assembly. *Journal of Manufacturing Science and Engineering* 144(8), 081009.